FIRST-LIGHT IMAGERY FROM SUOMI NPP VIIRS

BY DONALD HILLGER, THOMAS KOPP, THOMAS LEE, DANIEL LINDSEY, CURTIS SEAMAN, STEVEN MILLER, JEREMY SOLBRIG, STANLEY KIDDER, SCOTT BACHMEIER, TOMMY JASMIN, AND TOM RINK

Dramatic examples from first-light imagery, both single and multi-band, as well as the day-night-band, show that the 22-band sensor aboard the Suomi NPP satellite exceeds both requirements and expectations.

The launch of the Suomi National Polar-Orbiting Partnership (NPP) on 28 October 2011 marked a new generation of operational polar-orbiting spacecraft. Suomi NPP, which was renamed in January 2012 to honor "the father of satellite meteorology" Verner Suomi (Lewis et al. 2010), was originally called the National Polar-orbiting Environmental Satellite System (NPOESS) Preparatory Project (Lee et al. 2010), utilizing the same NPP initialism. NPP was originally considered a risk-reduction mission, but after the breakup of NPOESS, the Joint Polar Satellite System (JPSS) inherited NPP to become the prototype operational satellite anticipating the renamed JPSS-1 and -2 (Fig. 1) yet to be launched.

AFFILIATIONS: HILLGER AND LINDSEY—NOAA/NESDIS/STAR, Fort Collins, Colorado; KOPP—The Aerospace Corporation, El Segundo, California; LEE AND SOLBRIG—Naval Research Laboratory, Monterey, California; SEAMAN, MILLER, AND KIDDER—Cooperative Institute for Research in the Atmosphere, Colorado State University, Fort Collins, Colorado; BACHMEIER, JASMIN, AND RINK—Cooperative Institute for Meteorological Satellite Studies, University of Wisconsin—Madison, Madison, Wisconsin
CORRESPONDING AUTHOR: Donald W. Hillger, NOAA/NESDIS/STAR/RAMMB, CIRA-1375, Colorado State University, Fort Collins, CO 80523-1375
E-mail: don.hillger@NOAA.gov

The abstract for this article can be found in this issue, following the table of contents.
DOI:10.1175/BAMS-D-12-00097.1

In final form 6 December 2012
©2013 American Meteorological Society

The Visible–Infrared Imaging Radiometer Suite (VIIRS; please see sidebar for additional information), the primary imaging instrument on JPSS spacecraft, includes an expanded set of visible and infrared spectral bands (Table 1) to greatly improve upon its operational predecessor Advanced Very High Resolution Radiometer (AVHRR), as well as an enhanced-capability day/night band (DNB) (Lee et al. 2006) to improve upon the day/night imagery available from the Operational Linescan System (OLS) on the Defense Meteorological Satellite System (DMSP) series.

FIG. 1. Logo for the JPSS constellation, which includes the Suomi NPP satellite.

After a brief explanation of what is new with Suomi NPP, the following sections will provide dramatic examples of the improved capabilities of VIIRS imagery.

WHAT IS NEW AND IMPROVED WITH VIIRS ON SUOMI NPP? This article highlights VIIRS imagery, one of many environmental data records (EDRs) from VIIRS. Many additional EDRs are being developed and tested (sea surface temperature, cloud properties, ocean color, aerosol characteristics, etc.), but the imagery EDR has recently achieved the "beta" stage of maturity and is on its way to further levels of quality control. The examples presented here

Table 1. VIIRS bands and explanations. M = moderate-resolution bands; I = imagery resolution bands. M bands highlighted in pale yellow are available (by default) as EDRs in addition to sensor data records (SDRs). Components of true-color visible imagery are highlighted in red, green, and blue. M-band and I-band components of natural-color imagery are noted with R, G, and B.

VIIRS band	Central wavelength (μm)	Wavelength range (μm)	Band explanation	Spatial resolution (m) at nadir
M1	0.412	0.402–0.422	Visible	750 m
M2	0.445	0.436–0.454		
M3	0.488	0.478–0.488		
M4	0.555	0.545–0.565		
M5 (B)	0.672	0.662–0.682		
M6	0.746	0.739–0.754	Near IR	
M7 (G)	0.865	0.846–0.885		
M8	1.240	1.23–1.25	Shortwave IR	
M9	1.378	1.371–1.386		
M10 (R)	1.61	1.58–1.64		
M11	2.25	2.23–2.28		
M12	3.7	3.61–3.79	Medium-wave IR	
M13	4.05	3.97–4.13		
M14	8.55	8.4–8.7	Longwave IR	
M15	10.763	10.26–11.26		
M16	12.013	11.54–12.49		
DNB	0.7	0.5–0.9	Visible	750 m across full scan
I1 (B)	0.64	0.6–0.68	Visible	375 m
I2 (G)	0.865	0.85–0.88	Near IR	
I3 (R)	1.61	1.58–1.64	Shortwave IR	
I4	3.74	3.55–3.93	Medium-wave IR	
I5	11.45	10.5–12.4	Longwave IR	

will offer a good overview of VIIRS imagery products, though work continues on VIIRS imagery checkout.

The first VIIRS visible images from Suomi NPP became available on 21 November 2011, less than a month after launch of the satellite, followed by infrared images, available on 19 January 2012. VIIRS images have been spectacular, with finer (375 and 750 m at nadir) spatial resolution and multispectral (22 band) capabilities, not unlike those from the Moderate Resolution Imaging Spectroradiometer (MODIS), a key heritage instrument aboard the Earth Observing System (EOS) *Terra* and *Aqua* satellites. However, in addition to higher spatial resolution, VIIRS has visible capabilities for nighttime imaging using the DNB, at much better sensitivity and better spatial resolution than previously seen from OLS.

VIIRS imagery is a product in the sense that the images are calibrated and validated before they are made available to the public in Hierarchical Data Format version 5 (HDF5) format via the National Oceanic and Atmospheric Administration (NOAA)'s Comprehensive Large-Array Data Stewardship System (CLASS; www.class.ncdc.noaa.gov). VIIRS is parsed into single-band granules consisting of approximately 86 seconds of data each, requiring software to read the files, and image processing software

UNIQUE FEATURES OF VIIRS

Unique features of VIIRS, as compared with its predecessors:

- Finer spatial resolution for all bands (down to 375 m)
- Finer spatial resolution at swath edge in particular
- Wider (3,000 km) swath, leaving no gaps between orbits
- Day/night band enables visible light imagery under all natural and artificial illumination conditions

is needed to display the imagery. Useful packages for image manipulation include McIDAS-V (www.ssec.wisc.edu/mcidas/software/v/) and IDL (www.exelisvis.com/ProductsServices/IDL.aspx). VIIRS granules are accompanied by Earth-location information, which allows mapping the imagery into desired projections. Many qualitative uses of the imagery, some of which are provided as examples, are part of the validation of VIIRS.

FIRST-LIGHT IMAGES IN THE VISIBLE AND INFRARED. Among the unique capabilities offered by VIIRS, the spatial resolution of its infrared (IR) bands may be the most impressive. Both MODIS and AVHRR have IR resolutions of 1 km, so VIIRS's 375 m represent a significant improvement over previous instruments. This improvement is most evident when viewing small-scale features such as thunderstorm overshooting tops. Figure 2 shows a comparison between *Geostationary Operational Environmental Satellite-13* (*GOES-13*) band 4 (10.7 μm, 4-km resolution; Figs. 2a,b), MODIS 11.0-μm band 31 (1-km resolution; Figs. 2c,e), and VIIRS band I5 (11.45 μm, 375-m resolution; Figs. 2d,f). The convective complex shown in Fig. 2 was sampled by GOES at 0815 UTC, by MODIS at 0816 UTC, and by VIIRS at 0817 UTC.

An overshooting top is denoted by a blue circle in Figs. 2b–d, and the final two panels show extreme close ups over the circled regions from MODIS and VIIRS. The coldest brightness temperature of this feature from GOES, MODIS, and VIIRS was −79.7°C, −86.9°C, and −90.6°C, respectively. These differences are partly due to the smaller pixel sizes of the instruments with better resolution, with VIIRS providing the most accurate estimate of the actual emitting temperature of the thunderstorm overshooting top. VIIRS scanned the overshooting top 70 seconds after MODIS, so some evolution of the cloud top between the scans likely occurred. The relative pixel size of MODIS and VIIRS can be seen by comparing Figs. 2e and 2f.

MULTISPECTRAL IMAGERY (INCLUDING TRUE-COLOR IMAGE COMBINATIONS). VIIRS offers the requisite spectral bands to produce true-color imagery—a form of red-green-blue

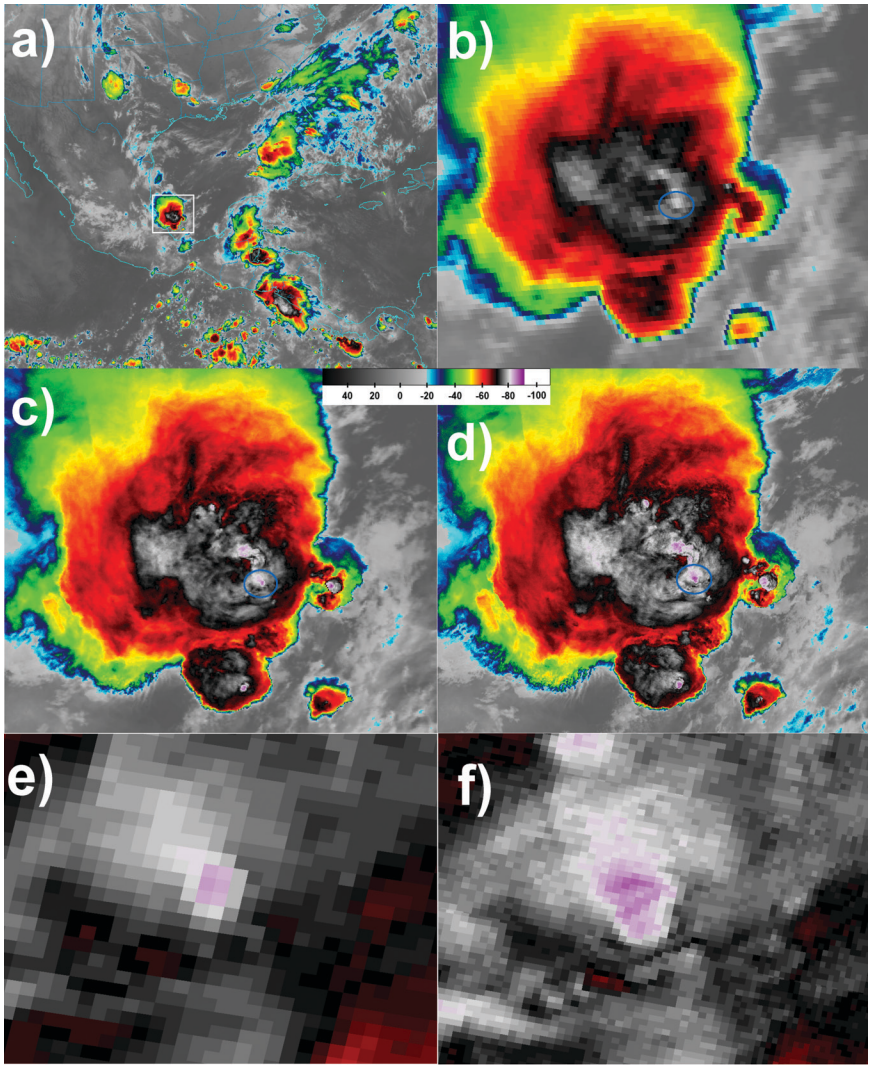

FIG. 2. (a) *GOES-13* 10.7-μm image from 0815 UTC 6 Jun 2012, (b) zoomed-in version of (a) over the highlighted thunderstorm complex in the southwestern Gulf of Mexico, (c) *Aqua* MODIS band 31 (11.0 μm) view of the same thunderstorm complex at 0816 UTC, and (d) NPP VIIRS band I5 (11.45 μm) view at 0817 UTC. An extreme close-up approximately covering the circled region from the MODIS image in (c) is shown in (e), and a similar close-up from VIIRS is shown in (f). The legend shows the brightness temperatures (°C).

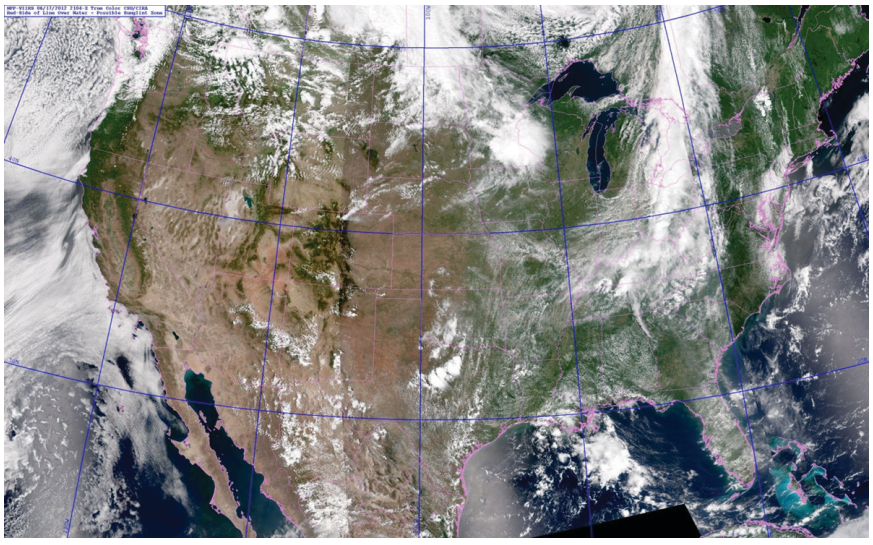

Fig. 3. Suomi NPP VIIRS true-color imagery from bands M3–M5, composited from three consecutive daytime passes on 17 Jun 2012, shows the continental United States and surroundings in vivid color detail.

composite imagery (e.g., d'Entremont and Thomason 1987) that attempts to reproduce the appearance of color photography. Presenting imagery in this way provides a familiar appearance to vegetated versus barren land surfaces, ocean features (including shallow-water regions and phytoplankton blooms), and atmospheric features (e.g., distinction between clouds, smoke, and blowing/drifting dust). The visually intuitive nature of this imagery makes it appealing to both novice and experienced satellite imagery users alike. VIIRS true-color processing, which entails an atmospheric correction (Ahmad and Fraser 1982) to remove atmospheric scattering and reveal surface details more vividly, has been adapted here from the National Aeronautics and Space Administration (NASA) MODIS algorithm.

Figure 3 shows an example of VIIRS true-color imagery over the continental United States. The scene is stitched together from three adjacent ascending passes of the Suomi NPP satellite on 17 June 2012. Vegetated surfaces over the Pacific Northwest, the Rocky Mountains, and the eastern United States contrast with the relatively dry/barren terrain of the eastern Great Plains and the desert Southwest. Shallow-water regions are apparent in the Bahamian shoals east of Florida, and signs of dark-green phytoplankton blooms are evident offshore of southern Baja California. The linear along-track-oriented regions of diffuse brightening over the oceans (Atlantic, western Gulf of Mexico, and Pacific) are due to sun glint. In the

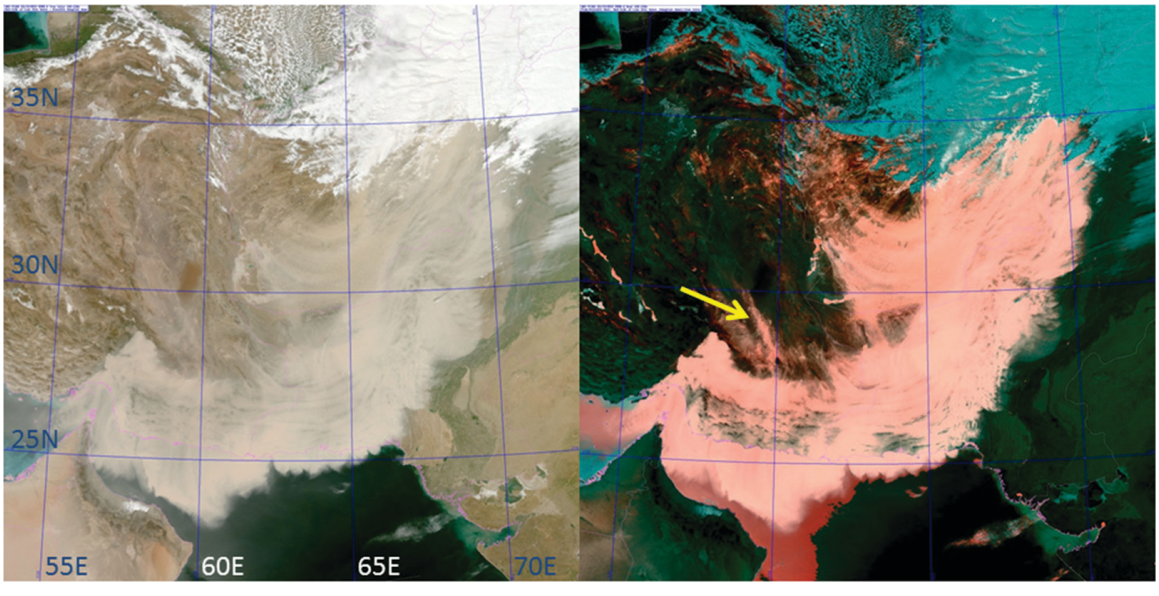

Fig. 4. Example of (left) Suomi NPP VIIRS true color and (right) enhanced dust (dust appears as pink, clouds in cyan, and land in shades of green) imagery. Images are from 0905 UTC 19 Mar 2012. The enhanced imagery is particularly useful for identifying dust over bright land surface backgrounds, such as the narrow plume indicated in the enhancement by the yellow arrow.

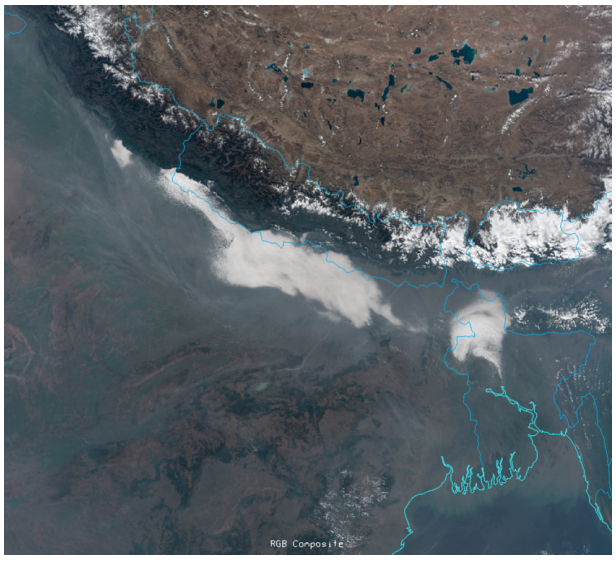

Fig. 5. VIIRS true-color image from bands M3–M5 over northern India and Tibet at 0725 UTC 14 Dec 2011. Note the large contrast in aerosol scattering between the cooler, drier, and shallower air mass to the north of the Himalayan chain and the warm, humid, and deeper air mass to the south.

future, VIIRS data will be used to train an algorithm that will permit the next-generation NOAA geostationary satellites (GOES-R series) to render true-color imagery from the Advanced Baseline Imager (ABI), despite the ABI's lack of a green band (Hillger et al. 2011; Miller et al. 2012).

Satellite imagery interpretation is particularly challenging when the feature under scrutiny blends in with the surface background. Blowing or drifting dust, composed of similar minerals as the surface background, is a particularly difficult example. Figure 4 shows an example of a false-color RGB enhancement (true color shown in left panel, for context) for a massive dust outbreak that occurred over parts of Iran, Afghanistan, and Pakistan on 19 March 2012 (the VIIRS pass captured the multihour event in progress at 0905 UTC). The detection capability was adapted from an algorithm described by Miller (2003) and developed originally on MODIS data. The enhancement enlists seven spectral bands from VIIRS spanning the visible, near infrared, and thermal infrared to portray areas of airborne dust in pink, clouds in cyan, and clear-sky land surfaces in green.

As an example of an atmospheric application of a VIIRS multispectral product, Fig. 5 is a true-color image over northern India and Tibet, with a large contrast in the atmospheric scattering between north and south of the Himalaya mountain chain. While certain VIIRS image products may focus specifically on aerosols, it is immediately obvious from the imagery alone that there is a much larger concentration of aerosols in the hazy and deeper atmosphere over India, compared to the less polluted and thinner air over Tibet, where surface features are much more easily discerned. This image also captures low clouds just south of the Himalayas.

Before leaving the VIIRS visible and infrared imagery, it is important to mention the ability to capture higher-resolution imagery at swath edge compared to heritage instruments such as MODIS and AVHRR. Through special processing of multiple detectors, the VIIRS footprint expansion at swath edge is only degraded by a factor of 2 instead of what would normally be a factor of 5 if uncompensated! Figures 6b

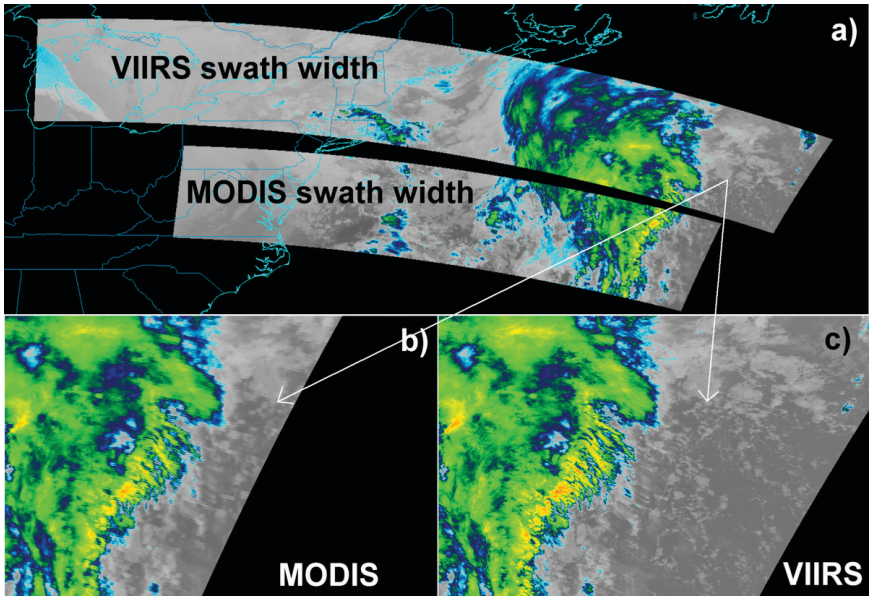

Fig. 6. Comparison showing (a) the difference in swath width between MODIS (band 31, 1-km resolution) and VIIRS (band 15, 11.45 μm, 375-m resolution) data from 0632 UTC 15 Feb 2012, and the relative difference in swath edge resolution between (b) MODIS and (c) VIIRS. Bowtie effects have been corrected for in both the MODIS and the VIIRS imagery. The color bar legend can be found in Fig. 2.

and 6c provide an edge of swath comparison between images from VIIRS and MODIS. From the color-enhanced cloud tops, the better spatial resolution of VIIRS at the edge of swath is apparent.

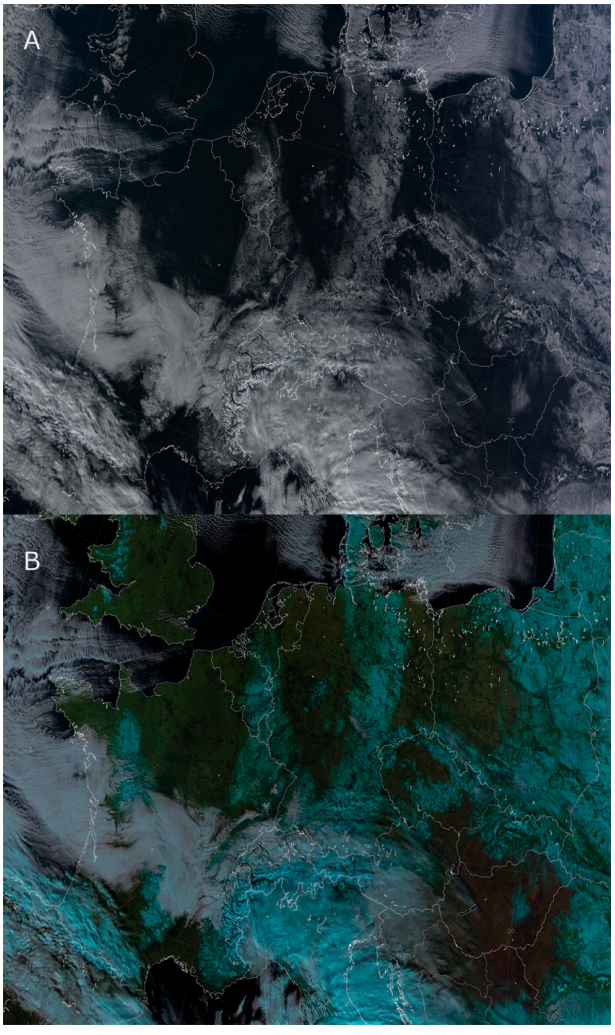

Fig. 7. Example of (a) VIIRS true-color composite and (b) natural-color composite of central Europe, taken 1211 UTC 1 Feb 2012. The natural-color composite easily distinguishes surface snow, which shows up as cyan. Ice clouds, primarily over Italy and southern France, also appear cyan, while liquid clouds show up a dirty white color, which allows for easy discrimination of cloud phase as compared with the true-color composite, where snow, liquid clouds, and ice clouds all appear white.

VIIRS also has a 3,000-km-wide swath, compared to 2,330 km for MODIS (see Fig. 6a for a VIIRS–MODIS comparison) and 2,800 km for AVHRR, with the result that complete coverage of Earth is obtained by VIIRS imagery, without the gaps seen between adjacent orbits in MODIS or AVHRR composite images of the world.

NATURAL-COLOR IMAGERY. VIIRS has the capability to produce both "true color" and "natural color" imagery. True-color composites have the advantage of closely representing what a human observer would see when looking down on Earth from space. Natural-color composites [natural-color imagery term was coined by Lensky and Rosenfeld (2008) and was first widely used by the European Organisation for the Exploitation of Meteorological Satellites (EUMETSAT; http://oiswww.eumetsat.org/IPPS/html/MSG/RGB/NATURALCOLOR/)] in many cases appear similar to true-color composites, although they provide additional information in the form of cloud phase discrimination and the discrimination of low clouds from ice and/or snow. Table 2 summarizes the bands that can be combined into true-color and natural-color imagery (Hillger 2008). In each case bands are combined via a three-color [red–green–blue (RGB)] combination, but only the first combination is true-color imagery, noted by the colored highlighting of the component bands.

The moderate-resolution bands M3 (0.488 μm), M4 (0.555 μm), and M5 (0.672 μm) observe radiances in the blue, green, and red portions of the visible spectrum, respectively, which, when combined, produce the true-color RGB composite. The high-resolution imagery bands I1, I2, and I3 constitute the natural-color RGB composite with band I1 (0.64 μm) as blue, band I2 (0.865 μm) as green, and band I3 (1.61 μm) as red. The same natural-color combination is also available from bands M5 (0.672 μm), M7 (0.865 μm), and M10 (1.61 μm).

Figure 7 shows an example of the true-color and natural-color composites over central Europe, taken 1211 UTC 1 February 2012. In the natural-color composite (Fig. 7b), ice and snow show up as a cyan color because of absorption in band I3 (1.61 μm) that is not

Table 2. Commonly used three-color (RGB) combinations of VIIRS bands.

Three-color (RGB) product	Red (μm)	Green (μm)	Blue (μm)
True color	M5 (0.672)	M4 (0.555)	M3 (0.488)
Natural color	M10 (1.61)	M7 (0.865)	M5 (0.672)
	I3 (1.61)	I2 (0.865)	I1 (0.64)

present at the shorter wavelength bands. Liquid clouds show up as white (or a dirty white), as they reflect more uniformly in each of the natural-color bands. This allows for the discrimination of ice clouds from liquid clouds. Surface ice and snow appear a more vivid cyan color as the absorption in band I3 (1.61 μm) is even greater than in the ice clouds. Vegetation, which shows up as green in both composites, provides a stronger signal in the natural-color composite because of increased reflection in band I2 (0.865 μm) compared with band M4 (0.555 μm). The oceans and other large bodies of liquid water appear much darker in the natural-color composite as they are not reflective in bands I1, I2, or I3.

The natural-color composite, in combination with the high spatial resolution of the bands that constitute it, may be useful in monitoring ice flows and associated ice jams in large rivers. Figure 8 shows a sequence of natural-color images of the Yukon River delta region in west-central Alaska during the spring of 2012. The first image (Fig. 8a), taken on 1 May 2012, shows the Yukon River to be completely ice covered. The third image (Fig. 8c), taken on 22 June 2012, shows the Yukon River to be ice free. In the second image (Fig. 8b), sections of the river, particularly the lower portion of the river near the delta region, have ice, while the upper portion of the river further inland is ice free. The transition from an ice-covered river to an ice-free river is of concern to many towns along the river, as the springtime breakup of ice across the river can lead to ice jams that present a significant flood risk.

FIRST-LIGHT DAY/NIGHT IMAGERY. An important new capability of VIIRS is low-light visible imagery at night, which is particularly useful when lunar illumination is present to illuminate surface and atmospheric properties in the same way as sunlight during the day. The day/night band (Lee et al. 2006) provides continuity and marked improvements to the OLS (e.g., Croft 1978) that has flown on the DMSP constellation since the 1960s. The DNB offers

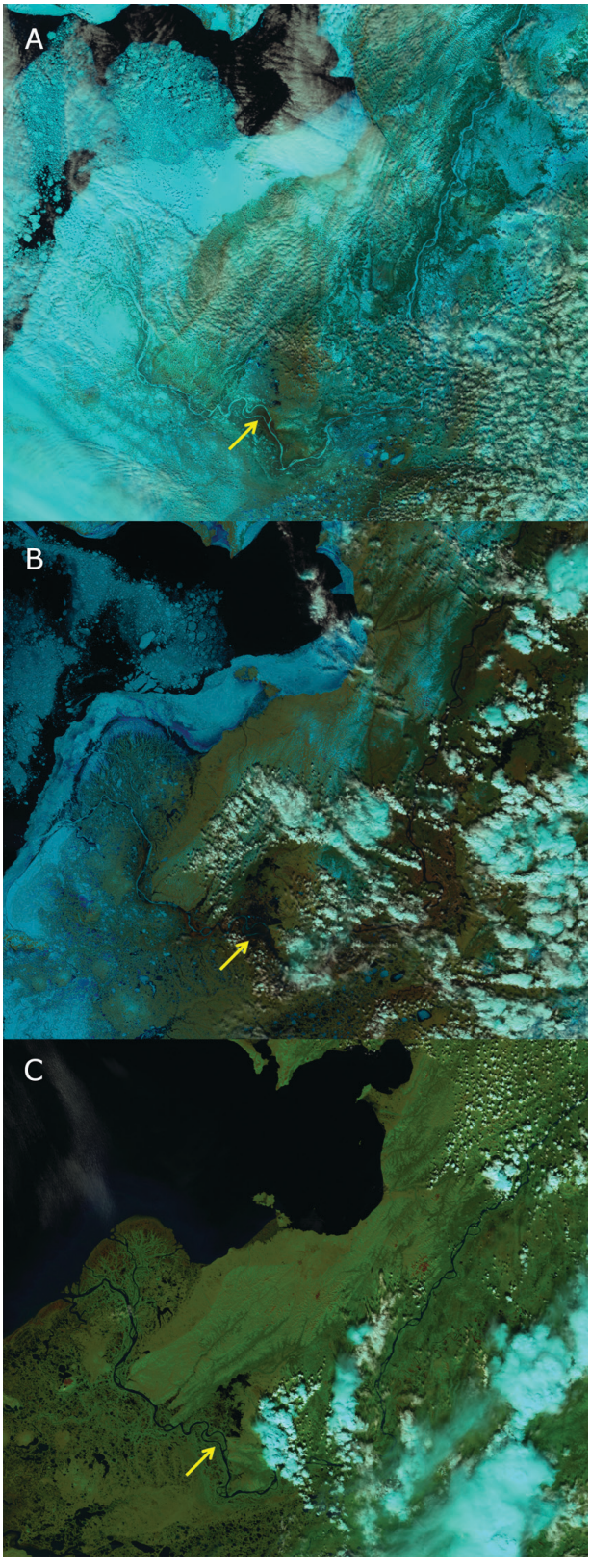

Fig. 8. VIIRS natural-color composite images of the Yukon River delta region of Alaska and Norton Sound. The Yukon River is visible from the top-right corner of each image southwestward down to the bottom middle and then it bends back northwestward toward the middle left, where it empties into Norton Sound. (a) The Yukon River is completely ice covered at 2238 UTC 1 May 2012. At (b) 2321 UTC 20 May 2012, ice is found only on portions of the river near the delta, and (c) the river is free of ice at 2322 UTC 7 Jul 2012. The yellow arrows indicate the farthest upstream extent of ice in (b) where evidence of flooding is found. Flooding is not apparent at this location in (a) or (c). The breakup of ice in Norton Sound over this time period is also visible.

nearly constant 750-m spatial resolution across the full 3,000-km-wide swath and operates three independent stages of gain (low/middle/high) to provide calibrated radiances at 14-bit radiometric resolution during the day, across the day/night terminator, and into the night side of Earth. Combined with the multiple near-infrared and thermal infrared bands on VIIRS (OLS provides only an 11.0-μm companion measurement), a truly new paradigm for multispectral nighttime applications is introduced, and for this reason the DNB represents arguably the most innovative component of NPP and the future JPSS constellation. DNB imagery has also been found to be useful even in no-moon conditions, way beyond the requirement to produce imagery down to quarter-moon illumination.

Figure 9 shows an example of nighttime low-light visible imagery from the VIIRS DNB collected during an active eruption of the Puyehue–Cordón Caulle volcano, bracketed in time by daytime true-color imagery from the *Aqua* MODIS satellite. In the nighttime image (expanded zoom), the ash plume is clearly evident by illumination from a full moon. The imagery sequence shows that the wind backed from southeasterly to northwesterly over the course of the predawn hours. In cases where such features reside close to the surface, thermal-infrared-based detection techniques (the only other nighttime imagery) may not provide reliable detection capability because of the thermal similarity of the features to the surrounding background. Here, the availability of visible light reflectance provides strong contrast, particularly in the case of low clouds, fog, smoke, or ash against low-albedo backgrounds such as water or dense vegetation. Discrete bright white patches in Fig. 9 are light emissions from human developments, and a discerning eye can detect light from the volcanic caldera itself—likely the visible light emissions from magma. Future application development will combine the DNB with other VIIRS bands to enable new RGB products. Quantitative property information from the calibrated DNB radiances is also possible using the predictive model of Miller and Turner (2009).

Figure 10 shows one example of the aurora borealis, as a bright swirl, over central Canada as viewed by the DNB during the early morning hours of 9 March 2012. A full moon occurred on 8 March 2012,

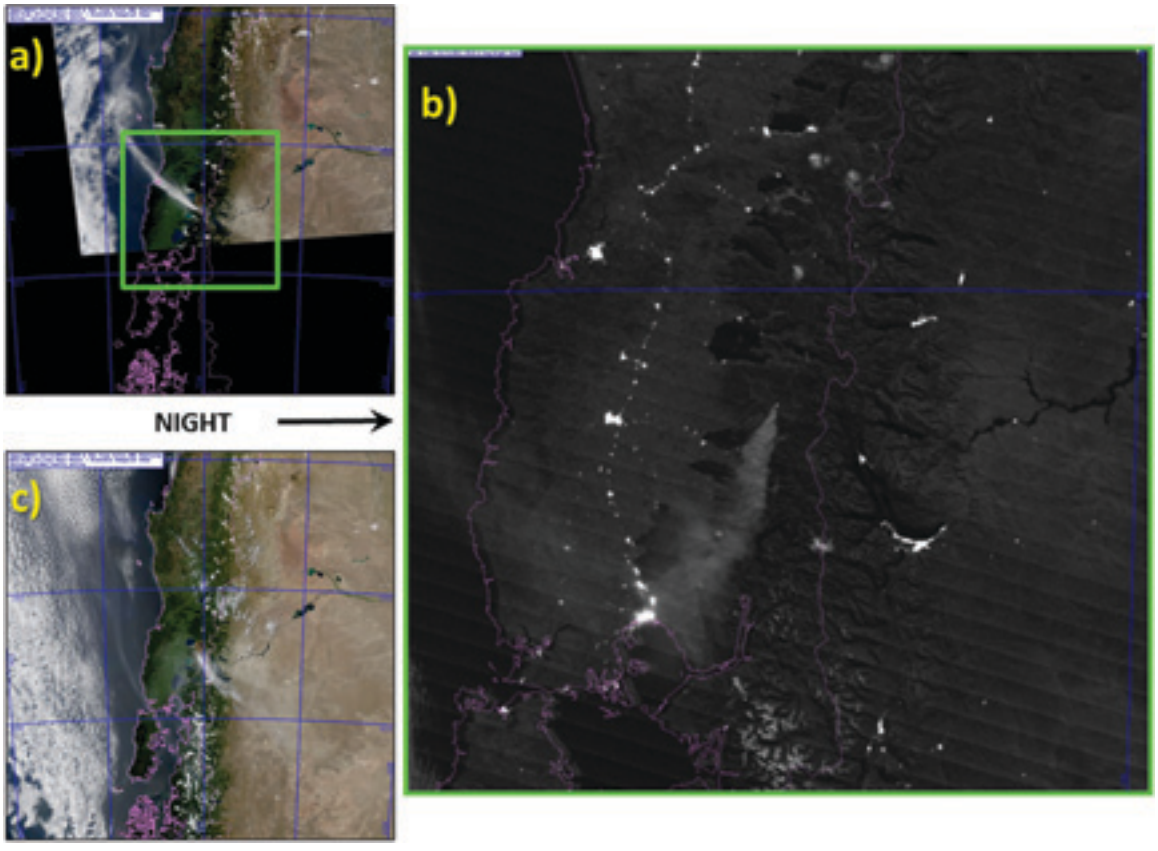

Fig. 9. Multisensor imagery sequence over the Puyehue–Cordón Caulle volcanic chain in Chile during an ongoing eruption, showing (a) *Aqua* MODIS at 1810 UTC 12 Dec 2011, (b) VIIRS DNB at 0510 UTC 13 Dec 2011 for the inset box region of (a), and (c) *Aqua* MODIS at 1850 UTC 13 Dec 2011.

enabling the DNB to distinguish many atmospheric and surface features. A band of high clouds is visible from southwestern Manitoba to northern Alberta, underneath which city lights are visible. More opaque clouds may be seen in southern and central Alberta. Ice-covered lakes are easily visible in cloud-free areas of Manitoba and Saskatchewan among the darker forests.

With the moon approximately 80% full, the DNB captured deep convection over Colombia and Venezuela during the early morning hours of 10 May 2012 (Fig. 11). Lightning shows up in DNB imagery as relatively large blocks of light in a nearly rectangular shape. As the instrument scans across the satellite track, bright transient flashes (e.g., lightning) appear in the along-scan (across track) direction as an individual streak of light in each sensor. The DNB has 16 different sensors that scan the swath simultaneously, and since lightning typically stretches over a large enough area to be detected by all of them, 16 different streaks line up next to each other. By the time the sensors have rotated back around for the next scan, the lightning flash has ended, producing abrupt edges in the direction along the satellite track. Note also in Fig. 11 that the moonlight is bright enough to cast shadows on the anvil clouds associated with the deep convective overshooting tops.

The DNB may also be used to identify wildfires at night. Figure 12 shows a DNB image of wildfires near the border of Montana and Wyoming in the northern high plains of the United States along with shortwave infrared brightness temperatures from 26 June 2012. Three wildfires are visible as light sources in the DNB (Fig. 12a) and as hot spots in the shortwave infrared band I4 (3.74 μm; Fig. 12b). These fires are identified as the Ash Creek fire, Cato fire, and an unnamed fire along Rocky Point Road near Gillette, Wyoming (Benoit 2012; Brown and Payne 2012). The Ash Creek fire eventually burned 1,010 km^2 and the Cato fire eventually burned 112 km^2. The third fire burned only 0.2 km^2 (20 ha), yet is easily visible in both bands shown in Fig. 12. Clouds are apparent in the shortwave infrared band I4 (Fig. 12b) that are not visible in the DNB (Fig. 12a). This is due to the fact that the moon had already

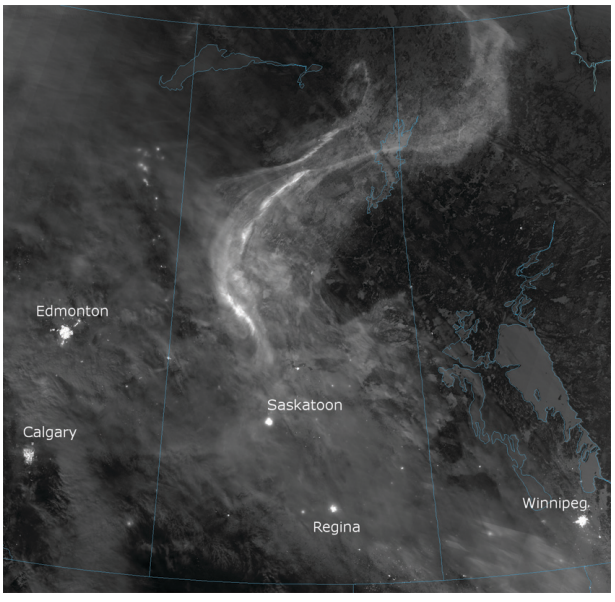

Fig. 10. VIIRS DNB image of the aurora borealis over central Canada from 0916 UTC 9 Mar 2012. Canadian provincial boundaries are shown with Saskatchewan in the middle of the image. With a full moon on 8 Mar 2012, clouds, snow, and ice-covered lakes are visible, along with city lights. Lights from major cities in the region have been labeled. The aurora extends from west-central Saskatchewan to northwestern Manitoba.

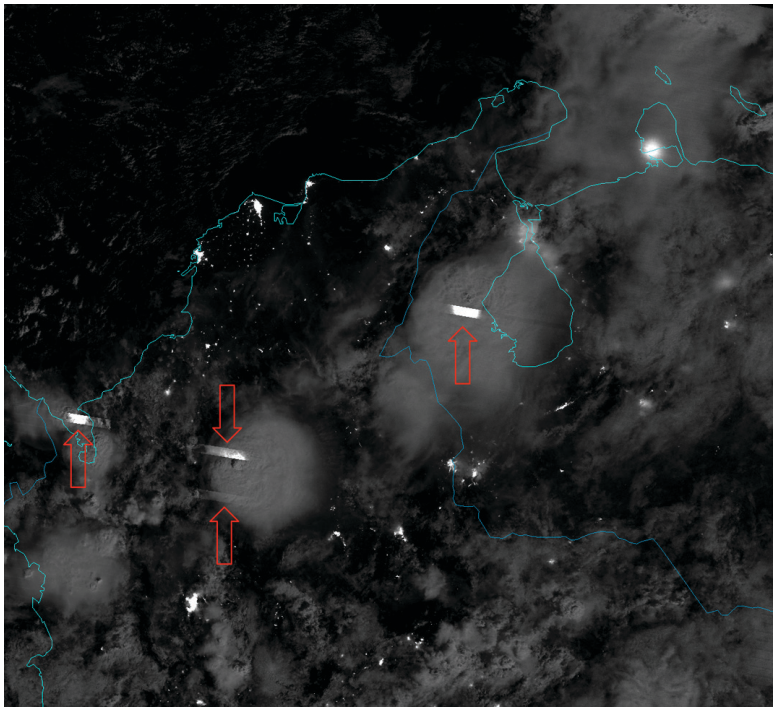

Fig. 11. VIIRS DNB image of lightning from thunderstorms over Colombia and Venezuela taken 0644 UTC 10 May 2012. Lightning strikes are identified by the red arrows. At the time this image was taken, the moon was approximately 80% full.

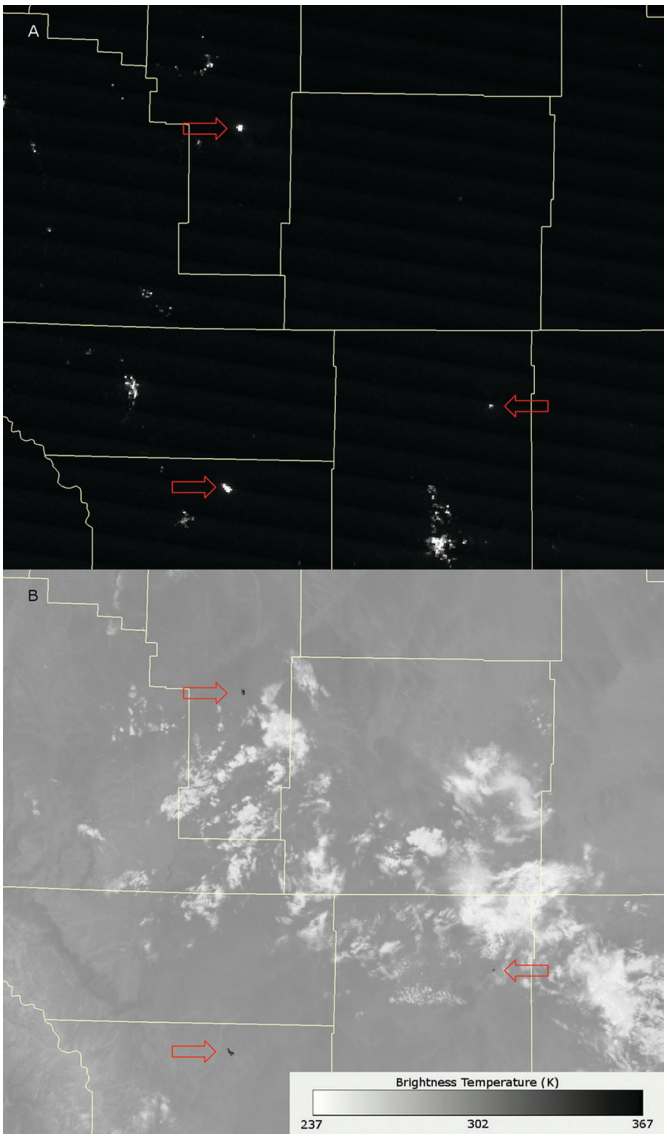

set over Montana and Wyoming by the time this image was taken. The NPP overpass was at 0835 UTC; the moon set on that date at 0637 UTC for that area. There was not enough moonlight for the DNB to detect clouds, but fires and city lights can be seen without any moonlight.

Finally, a mostly cloud-free VIIRS DNB image of the U.S. upper Midwest is shown in Fig. 13 at 0839 UTC 3 Sep 2012, as an example of not just lights from cities, but a large cluster of activity related to oil wells in the Bakken formation in northwestern North Dakota. The vast majority of the bright signal is due to illumination from the widespread "man camps" located throughout the region. These camps are literally small cities bustling 24 hours a day owing to all the drilling-related activities. DNB imagery has the ability to capture other man-made signatures, or lack thereof, including those related to power outages [Cooperative Institute for Meteorological Satellite Studies (CIMSS) satellite blog: http://cimss.ssec.wisc.edu/goes/blog/archives/10726].

SUMMARY AND CONCLUSIONS. The advent of Suomi NPP in late 2011 heralded a new generation in polar-orbiting remote sensing. The VIIRS image examples provided show the expanded capabilities of VIIRS on NPP, exceeding those of operational AVHRR and often those of MODIS. Examples were provided of visible and infrared imagery at

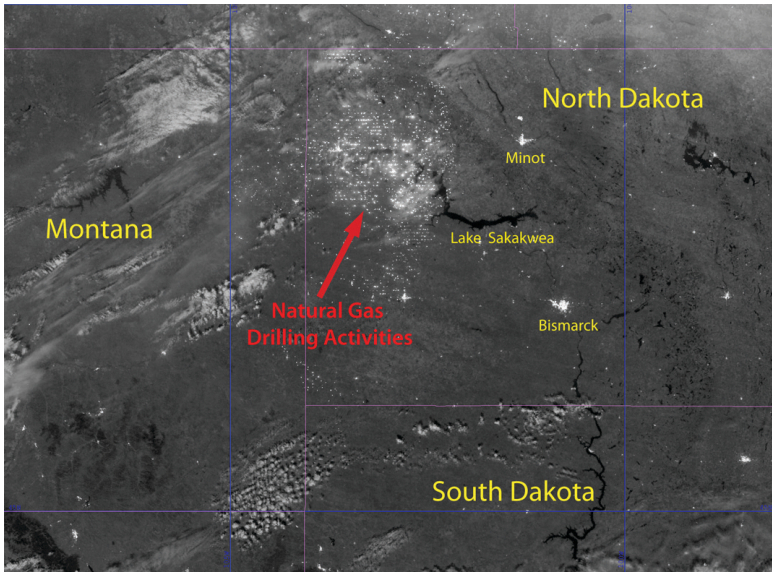

Fig. 12 (top). (a) VIIRS DNB image and (b) band 14 (3.74 μm) brightness temperatures of wildfires near the Montana–Wyoming state line, taken 0835 UTC 26 Jun 2012. Visible light and shortwave IR hot spots from the wildfires are indicated by the red arrows. County boundaries are also shown. The fires are identified as (clockwise from the top left) the Ash Creek fire, an unnamed fire along Rocky Point Road, and the Cato fire.

Fig. 13 (bottom). Mostly cloud-free DNB image over the U.S. upper Midwest at 0839 UTC 3 Sep 2012. Note the lights from major cities, as well as a large cluster of oil flare signatures in northwestern North Dakota from the recently developed Bakken formation.

increased spatial resolution (375–750 m) and various spectral band combinations, including true-color and natural-color imagery. Especially significant are the day/night band images with both increased resolution and much higher radiative sensitivity to low light levels. Images are possible day and night, and even in no-moon conditions, unlike those from the precursor OLS imagery.

ACKNOWLEDGMENTS. The authors would like to thank the following additional members of the STAR Imagery and Visualization Team (http://rammb.cira.colostate.edu/projects/npp/) for their contributions: Tim Schmit (GOES imagery liaison), Debra Molenar, Steve Finley, Chris Elvidge, Jeff Hawkins, Kim Richardson, Jeff Cetola, Keith Hutchinson, Steve Mills, and Calvin Liang. Funding for this work was provided by the JPSS Program Office and NOAA/NESDIS/STAR. The views, opinions, and findings contained in this article are those of the authors and should not be construed as an official National Oceanic and Atmospheric Administration (NOAA) or U.S. government position, policy, or decision.

REFERENCES

Ahmad, Z., and R. S. Fraser, 1982: An iterative radiative transfer code for ocean–atmosphere systems. *J. Atmos. Sci.,* **39,** 656–665.

Benoit, Z., cited 2012: Crews mopping up on fires in southeastern Montana, hope for full containment soon. [Available online at http://billingsgazette.com/news/state-and-regional/montana/article_f804f176-e01b-5a61-a503-46f95f48bdf4.html.]

Brown, K., and N. Payne, cited 2012: It's hot—After record-breaking days, is end in sight? [Available online at www.gillettenewsrecord.com/stories/Its-hot,73881.]

Croft, T. A., 1978: Night-time images of the Earth from space. *Sci. Amer.,* **239,** 68–79.

d'Entremont, R. P., and L. W. Thomason, 1987: Interpreting meteorological satellite images using a color composite technique. *Bull. Amer. Meteor. Soc.,* **68,** 762–768.

Hillger, D. W., 2008: GOES-R Advanced Baseline Imager color product development. *J. Atmos. Oceanic Technol.,* **25,** 853–872.

——, L. Grasso, S. Miller, R. Brummer, and R. DeMaria, 2011: Synthetic Advanced Baseline Imager true-color imagery. *J. Appl. Remote Sens.,* **5,** 053520, doi:10.1117/1.3576112.

Lee, T. F., S. D. Miller, F. J. Turk, C. Schueler, R. Julian, S. Deyo, P. Dills, and S. Wang, 2006: The NPOESS VIIRS day/night visible sensor. *Bull. Amer. Meteor. Soc.,* **87,** 191–199.

——, and Coauthors, 2010: NPOESS: Next-generation operational global Earth observations. *Bull. Amer. Meteor. Soc.,* **91,** 727–740.

Lensky, I. M., and D. Rosenfeld, 2008: Clouds-Aerosols-Precipitation Satellite Analysis Tool (CAPSAT). *Atmos. Chem. Phys.,* **8,** 6739–6753, doi:10.5194/acp-8-6739-2008.

Lewis, J. M., D. W. Martin, R. M. Rabin, and H. Moosmüller, 2010: Suomi: Pragmatic visionary. *Bull. Amer. Meteor. Soc.,* **91,** 559–577.

Miller, S. D., 2003: A consolidated technique for enhancing desert dust storms with MODIS. *Geophys. Res. Lett.,* **30,** 2071, doi:10.1029/2003GL018279.

——, and R. E. Turner, 2009: A dynamic lunar spectral irradiance dataset for NPOESS/VIIRS day/night band nighttime environmental applications. *IEEE Trans. Geosci. Remote Sens.,* **47,** 2316–2329, doi:10.1109/TGRS.2009.2012696.

——, C. Schmidt, T. Schmit, and D. Hillger, 2012: A case for natural colour imagery from geostationary satellites, and an approximation for the GOES-R ABI. *Int. J. Remote Sens.,* **33,** 3999–4028.

Science at Your Fingertips

AMS Journals are now optimized for viewing on your mobile device.

Access journal articles, monograph titles, and BAMS content using your iOS, Android, or Blackberry phone, or tablet.

Features include:

- **Saving articles for offline reading**
- **Sharing of article links via email and social networks**
- **Searching across journals, authors, and keywords**

And much more...

Scan code to connect to journals.ametsoc.org

Photos copyright University Corporation for Atmospheric Research, Gordon Farguharson and Harold Richter

AMERICAN METEOROLOGICAL SOCIETY